Investigations of pile-soil interaction under thermo-mechanical loading

Yi Rui[1], Mei Yin[2√]

[1]Dr Yi Rui

Centre for Smart Infrastructure & Construction, Department of Engineering, University of Cambridge, UK.

[2]Dr. Mei Yin

Schofield Centre, Department of Engineering

University of Cambridge, UK.

myin0915@gmail.com

[√] Corresponding Author: Department of Engineering, Trumpington Street, Cambridge, CB2 1PZ, UK.

myin0915@gmail.com

No. of words	6810
No. of tables	2
No. of figures	14

Abstract

Thermo-active piles that couple load bearing with ground source heat pump (GSHP) systems are one of the new technologies in geotechnical engineering. This paper investigates the pile-soil interaction behaviour of a thermo-active pile in overconsolidated London Clay by conducting a thermo-hydro-mechanical finite element analysis using an advanced soil constitutive model. Negative and positive excess pore pressures are computed around the pile during cooling and heating, respectively. However, the difference in the radial effective stress acting on the pile-soil interface between the cooling and heating stages is small, and the pile-soil interaction is governed by the shear mobilization associated with thermally induced cyclic movements of pile expansion and contraction. During the first cooling stage, the shear stress at a small portion in the upper part of the pile reaches close to the yield values, which leads to an additional settlement about 3 mm from the original mechanical load induced settlement of 2 mm. The shear stress in subsequent heating and cooling cycles are much smaller than the ultimate shear stress values, because of the heavily overconsolidated nature of the London clay.

Keywords

Thermo-hydro-mechanical analysis; thermo-active pile; finite element

1 Introduction

Domestic heating and cooling demand accounts for 50% of America's residential energy consumption (Caulk, et al. 2016). As the global energy demand is forecast to increase, unless renewable technologies are implemented on a larger scale, the world will be even more reliant on fossil fuels, and will be further exposed to global energy price fluctuations. The Ground Source Heat Pump (GSHP) is a technology which offers an alternative energy solution that uses geothermal energy for space heating and cooling in a domestic and commercial market, and their coupling to building foundation structure (piles/walls) not only reduces installation costs, but also saves underground space. Thermo-active pile is one such system, with a pipe network installed in the structural piles of a building, and the working fluid is circulated through the pipes to absorb and transport the geothermal energy from the ground. Since concrete has excellent thermal conductivity and good storage properties, foundation piles are an ideal medium for geothermal energy.

The first thermo-active pile was implemented in Austria in the 1980's (Brandl 2006). Since then it has spread all over the whole world (e.g. Koene et al. 2000; Suckling & Smith 2002; Pahud and Hubbuch 2007; Gao et al. 2008; Adam and Markiewicz 2009; Amatya et al. 2012). While this technology is now being employed more routinely and is starting to be represented in codes and standards (e.g. NHBC 2010; GSHPA 2012), there is still scope for improving design and analysis methods in both thermal aspect (e.g. Loveridge and Powrie 2014; Abdelaziz and Ozudogru 2016; and Caulk et al. 2016) and thermo-mechanical aspect. (Bourne-Webb et al. 2009; Knellwolf et al. 2011; Amatya et al. 2012; Suryatriyastuti et al. 2014; Chen et al. 2016). This paper focused on the latter case.

The thermo-active pile and surrounding soil expand and contract during heating and cooling, respectively, but to different degrees. (Bourne-Webb et al. 2009) Hence, the thermal influence on the pile-soil interaction behaviour must be quantified for use in engineering practice. A qualitative framework has been proposed by Bourne-Webb et al. (2009) and Amatya et al. (2012) to describe the mechanism of pile expansion/contraction due to temperature variation. Within this framework, load-transfer approach was put forward for the analysis of the thermo-mechanical response of thermo-active piles. Knellwolf et al. (2011) used this method to assess the effects of temperature changes on pile behavior. Some conclusions were formulated on concrete failure, mobilization of the shaft friction and base resistance during the operation of the heat pump. Suryatriyastuti et al. (2014) presented a soil–pile interaction design method of a thermo-active pile based on a load transfer approach, which can be used to predict the change in pile axial stress and shaft friction induced by temperature variations. Using the same approach, Chen et al. (2016) assessed the axial strains, axial stresses, and displacements thermo-active piles under thermo-mechanical loading in various soil deposits. However, the load-transfer approach only consider the thermally induced expansion and contraction of pile, but neglect the effect of temperature variation on the soil. Hence, this simplified approach may have inaccurate estimate of the thermo-active pile performance.

To avoid such limitation, a number of research has been done on the finite element analysis of the thermo-mechanical performance of thermo-active piles (Dupray et al. 2014; Olgun et al. 2014; Wang et al. 2015; Saggu and Chakraborty, 2015; Bourne-

Webb et al. 2016). Laloui et al. (2006) performed both experimental and coupled multi-physical finite element modelling on thermo-active pile. The proposed FE model is able to reproduce the most significant thermo-mechanical effects. Di Donna and Laloui (2015) used finite element method to simulate both a single and a group of thermo-active piles, leading to the conclusion that both the thermally induced displacements and stresses need to be taken into account in the design of thermo-active piles. Rotta Loria et al. (2015) examined the impact of thermal and mechanical load cycles on the mechanical behaviour of thermo-active piles in saturated sand. The results show that heating loads cause additional stress and displacement in thermo-active piles, and increase the mobilization and end-bearing capacity to a large extent. Suryatriyastuti et al. (2016) used a nonlinear cyclic plasticity model to show that the long-term pile capacity would decrease with cycles due to repetitive stress reversals.

Most of these studies were performed using a thermo-mechanical anlaysis based on a fully drained assumption (Brandl 2006 and McCartney et al. 2017). This is partly because of the high permeability of soils under investigation in the particular studies, and partly because of the long time operation of GSHP system. However, for some soil with extremely low permeability, like London Clay, the performance of thermo-active piles lie somewhere between the perfectly drained and undrained conditions. During the winter cycle (soil cooling), both the soil skeleton and the pore fluid contract. Due to the difference in the thermal contraction coefficients of the soil skeleton and the pore fluid, negative excess pore pressure is generated, and the total stress acting on the pile may change as a result (Campanella and Mitchell 1968). During the summer cycle (soil warming), the soil is heated, so the opposite trend is to be expected. The soil skeleton and the pore fluid expand, and positive excess pore pressure develops. Hence, a fully coupled thermo-hydro-mechanical analysis is needed for the investigations of pile-soil interaction in low-permeability soil under thermo-mechanical loading.

This paper investigates the pile-soil-pore fluid interaction in a specific case of the Lambeth College thermo-active pile installed in heavily overconsolidated and low-permeability London clay (Bourne-Webb et al. 2009; Amatya et al. 2012). A thermo-elasto-plastic advanced critical state model was implemented into a coupled thermo-hydro-mechanical finite element code. A coupled thermo-hydro-mechanical (THM) analysis of the test pile was performed to calibrate the model parameters against the results of the mechanical and thermal cycles applied on the test pile in the relatively short duration of a few weeks.

2 Mechanics of THM coupled processes

Based on the theory of continuum mechanics, a number of assumptions have been adopted to develop the coupled thermo-hydro-mechanical model for deformable porous geological media:

(1) The soil is treated as fully saturated porous medium. The voids of the solid skeleton are filled with liquid water.

(2) Coexisting fluid components and solid are assumed to be at the same temperature.

(3) Considering there is no ground water flow and the poor permeability of soil in the model, heat conduction is the main mean of heat transfer considered in this problem.

The saturated porous medium, in the context of theory of mixtures, is viewed as a mixed continuum of three independent overlapping phases. Its conservation equation can be obtained according to principles of continuum mechanics.

(1) Balance of linear momentum

$$\nabla \cdot (\boldsymbol{\sigma} - \mathrm{p}\mathbf{I}) + \rho\mathbf{g} = \mathbf{0} \tag{1}$$

Where $\boldsymbol{\sigma}$ is the stress tensor, p is the pore pressure, I is the identity tensor, $\mathbf{g}$ is the gravity acceleration vector. The component form of $\nabla \cdot \boldsymbol{\sigma}$ with the base vectors $\boldsymbol{e_i}$ can be written in the component form as

$$\nabla \cdot \boldsymbol{\sigma} = \frac{\partial \sigma_{ji}}{\partial \mathrm{x}_j} \boldsymbol{e_i} \tag{2}$$

A thermo-elasto-plastic advanced Cam-Clay Model is applied in this model. In this model,

$$\mathrm{d}\boldsymbol{\sigma}' = \mathbf{D^{ep}} : \mathrm{d}\boldsymbol{\varepsilon} + \mathbf{D^{Tep}} \mathrm{dT} \tag{2}$$

where, $\boldsymbol{\varepsilon}$ is the strain tensor, $\mathbf{D^{ep}}$ is the fourth-order elasto-plastic material tensor, and $\mathbf{D^{Tep}}$ is the second-order thermo-elasto-plastic material tensor with reference to temperature T. These two tensors can be derived from the elastic modulus, yield function and flow potential of the thermo-elasto-plastic model (Laloui and Cekerevac 2003). The details of this model are discussed in Appendix A. The double contraction of $\mathbf{D^e}$ with $\mathrm{d}\boldsymbol{\varepsilon}$ can be written in the component form as,

$$\mathbf{D}^{\mathrm{ep}} : \mathrm{d}\boldsymbol{\varepsilon} = \mathrm{D}^{\mathrm{ep}}_{\mathrm{ijkl}} \mathrm{d}\varepsilon_{\mathrm{kl}} \tag{6}$$

(2) Pore water flow in soil

$$\nabla \cdot \left(-\frac{\mathrm{k}}{\mathrm{r_w}} (\nabla \mathrm{p} - \rho \mathbf{g}) \right) + \div \dot{\mathbf{u}} + \frac{\mathrm{n}}{\mathrm{K_w}} \frac{\mathrm{dp}}{\mathrm{dt}} - \mathrm{n}\alpha_{\mathrm{Tw}} \dot{\mathrm{T}} = 0 \tag{3}$$

k is the permeability coefficient, $\mathrm{r_w}$ is the unit weight of water, ρ is the density of water, ∇p is the gradient of p, $\mathbf{u}$ is the displacement vector of soil skeleton, $\mathrm{K_w}$ is the bulk modulus of water, n is the porosity of soil, α_{Tw} is the heat expansion coefficient of water ,$\div \dot{\mathbf{u}}$ is the trace of the gradient of $\dot{\mathbf{u}}$, which can be written as,

$$\div \dot{\mathbf{u}} = \sum_{\alpha=1}^{3} \frac{\partial \dot{u}_i}{x_i}$$

(3) Heat transfer in soil

$$-\nabla \cdot \left(D_{sw}^{H} \nabla T\right) + c_{sw}\, \dot{T} = Q_T \qquad (4)$$

D_{sw}^{H} is the heat conductivity of saturated soil, c_{sw} is the thermal capacity of saturated soil, Q_T is the heat source term.

3 Lambeth College thermo-active pile test

The purpose of the Lambeth College thermo-active pile test by Bourne-Webb et al. (2009) was to investigate the behaviour of a thermo-active pile installed in London Clay over different temperature cycles whilst under thermal and physical loading for an extended period of time, albeit short in comparison to the actual operation of a GSHP. The main test pile had a diameter of 610 mm (top 5 m) and 550 mm (below 5 m from the top) and a length of 23 m. One heat sink pile was installed some distance away from the main test pile to discharge or extract energy obtained from the main test pile. Figure 1(a) shows a schematic layout of the test components and the instrumentation details of the main test pile. A distributed Optical Fibre Sensing (OFS) System and other conventional instruments such as conventional vibrating-wire strain gauges and thermal couples were used to monitor the temperature and strain changes throughout the test. The applied physical load at the pile head, the pile head movement, the ambient air temperature and the input and output temperature of the fluid in the heat pump system were recorded during the test period, which lasted for seven weeks. Further details of the test can be found in Bourne-Webb et al. (2009) and Amatya et al. (2012).

The soil profile is shown in Figure 1(b). The top 1 m of superficial soil is Made Ground. This is underlain by river terrace deposits to a thickness of 3 m, followed by London Clay. The ground water table was measured at about 3 m bgl. The ground temperature on the site ranged from 18℃ to 20℃, which is roughly 3℃ to 5℃ higher than the average range of the ground temperature in London. It is believed that the temperature was raised due to heat radiated from the surrounding congested London underground tunnels (Bourne-Webb et al. 2009).

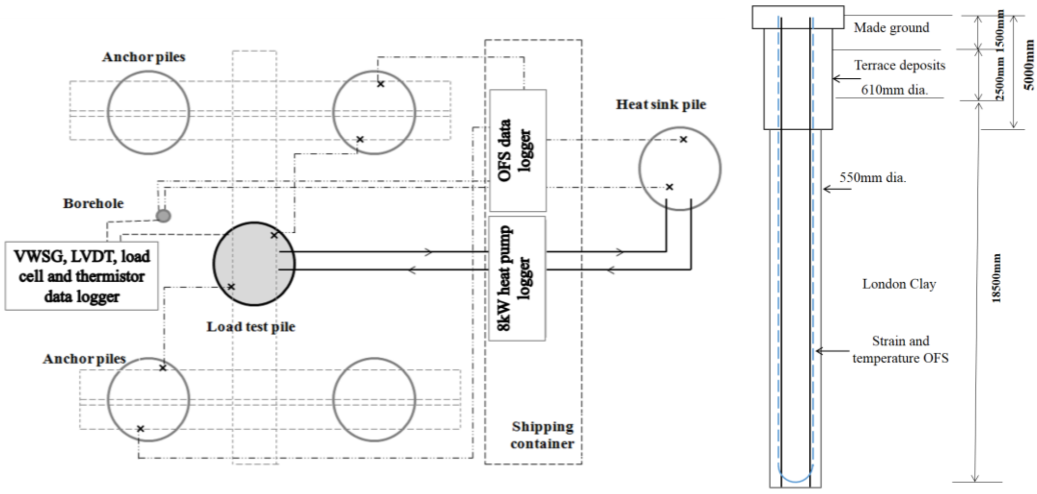

(a) (b)

Figure 1. (a) Schematic layout of test components from the thermo-active pile project at Lambeth College; (b) Distribution of OFS components in the test pile (after Bourne-Webb et al. 2009)

Before commencing the thermal test, the pile underwent two mechanical loading cycles of up to 1800 kN and then zero to 1200 kN, to test its behaviour under mechanical loading only, as shown in Figure 2(a). After this, the thermal loading cycles were applied. Figure 2(b) shows the pile temperature of the main test pile over time. Pile cooling commenced first. The temperature reached zero within 10 days and was kept constant at this temperature for 25 days. Heating was subsequently applied for 11 days. The temperature of the pile rose up to 37 ℃. However, the heating was interrupted for 2 days due to power failure. After the system recovered, the pile temperature was kept at about 31–34 ℃ for 7 days. After the first heating stage, several cooling and heating cycles were applied with a change in temperature of about 25 ℃. The magnitude of the temperature changes adopted in this testing programme is considered to be the maximum experienced in the actual operation of a GSHP, which sees an average change of about 20 ℃. The test was intended to examine the extreme case in terms of its thermo-mechanical response.

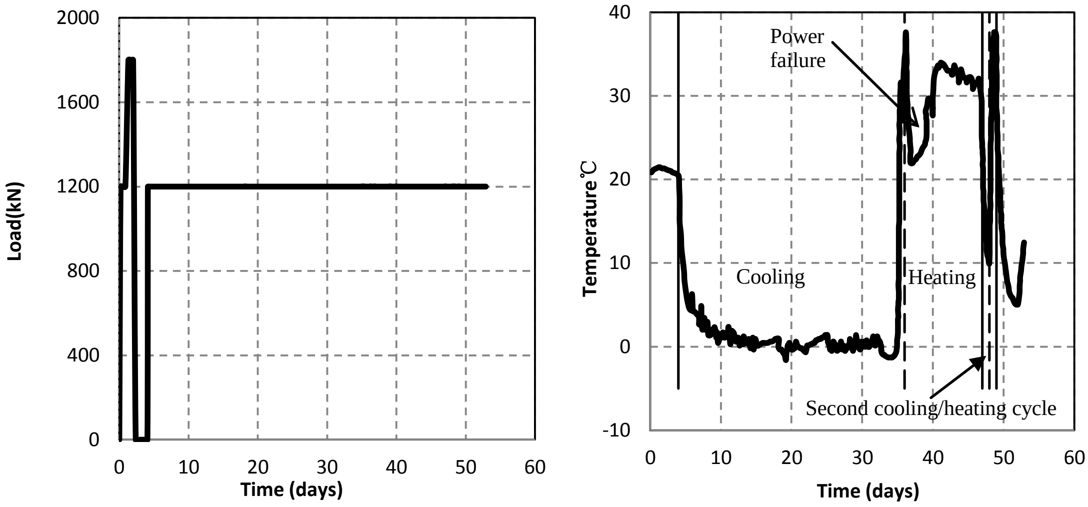

(a) (b)

Figure 2. (a) Load control applied at the pile head; (b) Temperature changes of the test pile over time at 9 m below ground level (Bourne-Webb et al. 2009)

The rate of heating in the Lambeth College thermo-active pile test performed by

Bourne-Webb et al. (2009) was faster than the rate of heating that would be encountered during typical operation of a thermo-active pile as described in Brandl (2006) and McCartney et al. (2017). This may lead to an undrained effect observed in the short term thermal response test that may not be observed during operation of some other thermo-active piles.

4 Finite element model

The finite element THM simulation of the pile installation as well as the operation of the GSHP was conducted using an in-house finite element code developed at the University of Cambridge (Rui, 2014). The ground model includes three layers at different depths: Made Ground, Terrace Gravel and London Clay. A quarter of the pile and the surrounding ground were modelled, as shown in Figure 3. The diameter of the top part of the pile is 610 mm, and decreases to 550 mm below an elevation of -5 m. The radius of the whole soil model is 8 m, incorporating three parts: Made Ground, Terrace Gravel, and London Clay. In this paper, the pipe network installed in the structural piles was not simulated. Instead, the temperature of whole pile was set as variable values as shown in Figure 2(b) in the FE analysis. The boundary conditions are also listed in Figure 3.

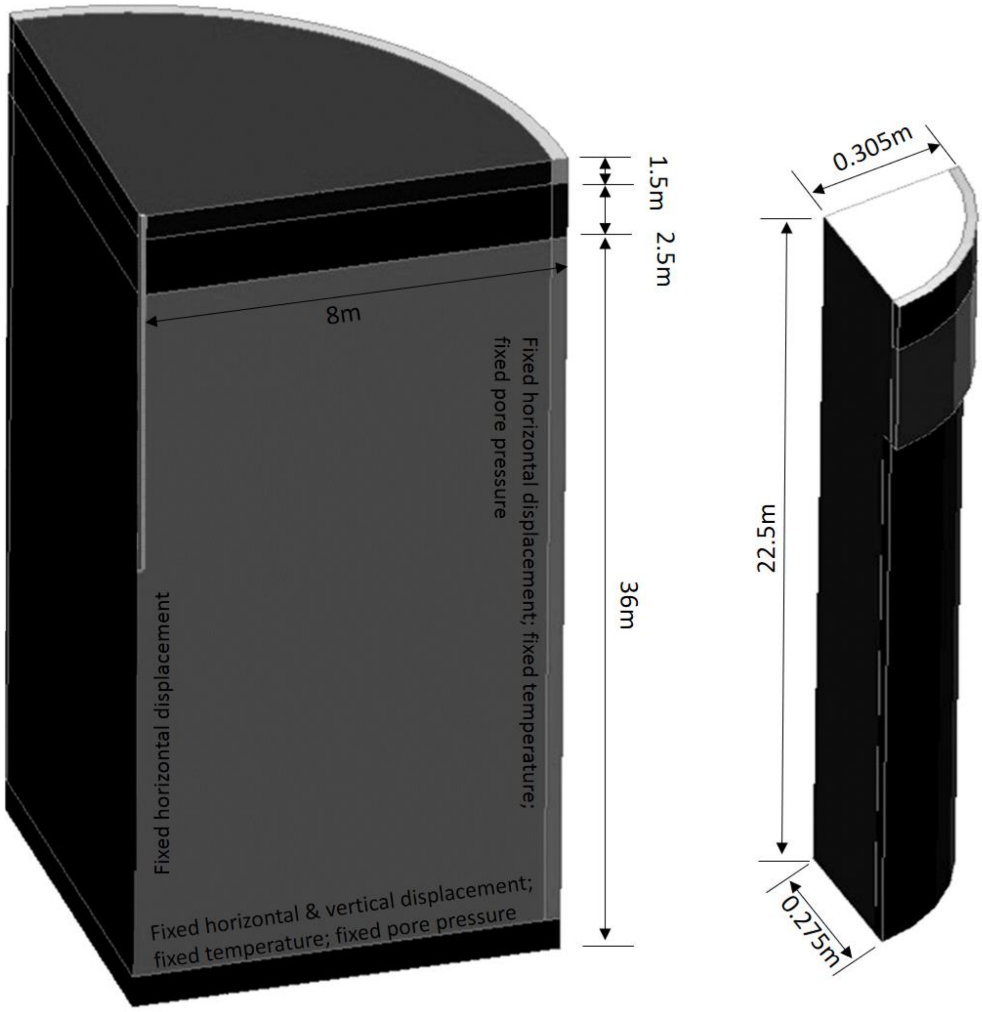

(a) (b)

Figure 3. Model layout (A quarter of the pile): (a) soil and pile; (b) pile

Modelling of the soil is done using the thermo-hydro-mechanical coupled model for porous media, as described in section 2, since it contains problems in which the various physical domains overlap. In the subsurface, soil deformation is associated with changes of pore pressure. Seepage flow along with the transfer of pore pressure influences the effective stress of soil skeleton. Temperature variation causes thermal deformation of both soil skeleton and pore fluid water. An anisotropic thermo-elasto-plastic advanced critical state model was used for all the soils. The details and parameters of the model are given in Appendix A.

The thermal properties of the soil were taken from the typical values in the design of ground source heat pump systems (Amis et al. 2008). There is limited data available on the thermo-mechanical properties of different soils. In this study, model calibration was performed by varying the thermo-mechanical model parameters so that the simulation results were similar to the field test data according to factors such as the pile settlement and distributed strain profile.

The temperature of pore fluid water is assumed to equal the temperature of the solid, and the linear thermal expansion coefficient of water was $70\ \mu\varepsilon/℃$. The pile concrete Young's modulus was 40 GPa, whereas the linear thermal expansion coefficient was $8.5\mu\varepsilon/℃$ (Bourne-Webb et al. 2009). In addition The linear thermal expansion coefficient was $20\mu\varepsilon/℃$, which was obtained from back-calculation of the field measurements by Bourne-Webb et al. (2016). In addition, London Clay has a low permeability coefficient $2 \times 10^{-11}\mathrm{m/s}$ (Wongsaroj, 2005; Laver, 2010). The model parameters for each material that were used for the simulations are summarized in Table 1.

Table 1 Model parameters

Parameters	**Pile**	**Made Ground (MG)**	**Terrace Gravel (TG)**	**London Clay (LC)**
Model	Elastic	Thermo-elasto-plastic (see Appendix A)	Thermo-elasto-plastic (see Appendix A)	Thermo-elasto-plastic (see Appendix A)
Elastic properties	G=16.7GPa $\nu = 0.2$	-	-	-
Unit weight	25.0	20.0	20.0	20.0

(kN/m^3)				
Thermal conductivity (W/(m.K))	2.37	1.8	1.8	1.5
Thermal capacity kJ/ m^3K	2400	3200	3200	3200
Thermo-elastic Expansion (με/℃).	8.5	20.0	20.0	20.0
Permeability (m/s)	-	$2x10^{-7}$	1×10^{-3}	$2x10^{-11}$

Following the actual procedure of the field test, the THM simulation was divided into the following six steps: (1) initial state, (2) wish-in place pile installation, (3) the first mechanical loading to 1800 kN, as shown in Figure 2(a), (4) the unloading stage, (5) the second mechanical loading to 1200 kN, as shown in Figure 2(a), and (6) the cooling and heating cycles (day 4 – day 49), as shown in Figure 2(b). In this model, initial stress conditions assumed the coefficient of earth pressure coefficient K0, was 1.0 (Bourne-Webb, 2016), and OCR of London clay was 18 (Yimsiri, 2001). The physical load is applied on the top of pile, and the displacement boundary condition is determined as horizontal displacement fixed for the side boundary and both vertical displacement fixed for bottom boundary, as shown in Figure 3. Initial thermal conditions assumed the constant initial temperature of 20 ℃, which was maintained on the bottom and side boundary. To simulate thermal loading, the nodal temperature of whole thermo-active pile was set as the values listed in Figure 2(b).

5 Results and discussion

5.1 Thermal response

Figure 4 shows the temperature contours in the soil during the operation of the field test. The zone of influence of the first cooling stage propagated radially with time (Figure 4 (a)). At the initiation of the heating stage, the temperature around the pile increased and then heat propagated radially with time (Figure 4 (b)). Similar patterns were observed in subsequent temperature cycles (Figure 4 (e & f)). The temperature change was rather uniform along the pile depth. The soil temperature below the pile base was also influenced by the change in temperature.

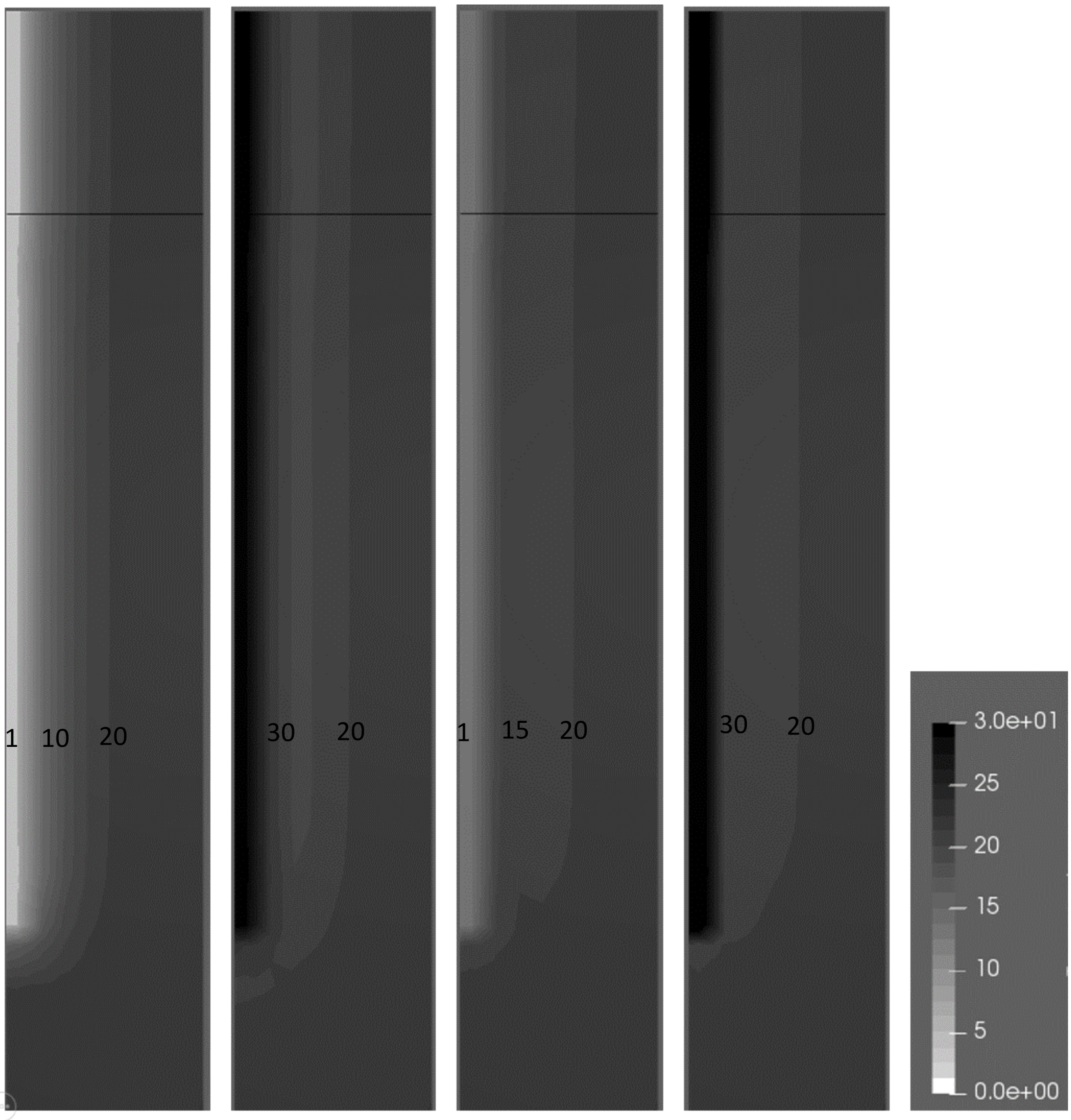

(a) (b) (c) (d) (e) (f)

Figure 4. Contours of changes in temperature(unit: ℃): (a) at the end of first cooling; (b) at the end of first heating; (c) at the end of second cooling; (d) at the end of second heating.

5.2 Pile displacement

The computed pile displacement at the top of the pile is compared to the field measurements in Figure 5. The pile was first subjected to a working load of 1800 kN, and the settlement was about 3 mm. After the load decreased to 0 kN, the pile head rebounded. The simulation gave 1.3 mm of residual settlement, whereas the actual residual settlement was 0.9 mm. The pile was reloaded to 1200 kN and the resulting computed settlement was 2.5 mm, which is similar to the actual settlement of 2.2 mm.

The first cooling stage began after reloading the pile to 1200 kN. The settlement was 4.5 mm during the first ten days of cooling, caused by the contraction of both the pile and the soil. After this, the settlement increased to 5.0 mm during the 30 days cooling period. This was due to the contraction of the ground as the cooling front propagated radially.

During the heating stage, the pile expanded and the pile settlement decreased to about 2.7 mm. There was an interruption to the heating, which increased the computed settlement to 4 mm. The actual settlement was 5 mm. After the heating resumed, the settlement rebounded back to about 2.7 mm. After the first cooling and heating stages, another cooling and heating cycle was simulated. The model results closely matched the monitoring data. As described earlier, the model parameters (especially the thermal-mechanical part) were calibrated to match the displacement, strain and temperature data.

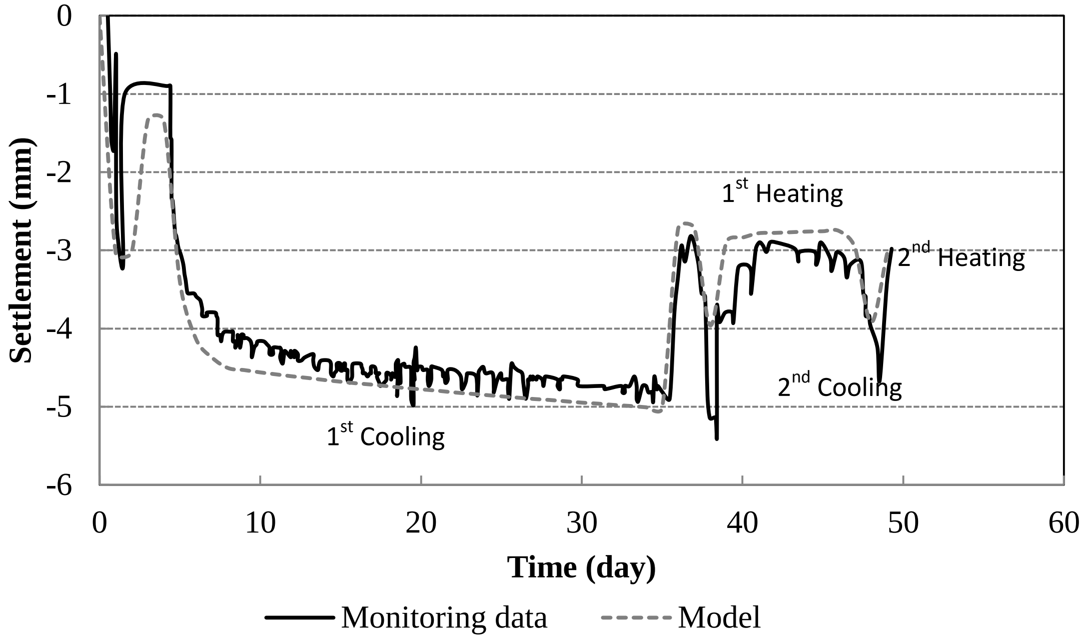

Figure 5. Settlement of the thermo-active pile

5.3 Pore pressure response

Figure 6 shows the excess pore pressure profiles of the soil elements adjacent to the thermo-active pile. At the 1200 kN loading stage, the excess pore pressures in the London clay next to the pile interface were positive. In particular, there was a relatively large increase in excess pore pressure at a depth of 5 m. This is where the pile diameter reduced from 610 mm to 550 mm, creating a partial end bearing geometry. Some load transfer to the soil occurred at this location, resulting in this small increase in excess pore pressure compared to the other parts of the pile. This is schematically illustrated in Figure 7. At the base, excess pore pressure in the soil existed due to the end bearing load. In addition, the thermally induced excess pore water pressure divided by the initial effective stress is about 5%-10% for every 10°C change in temperature, which is a little bit lower than the similar results (10%-20%) in undrained heating test for different soils summarized by Ghaaowd et al. (2015).

This is due to the partial completion of soil consolidation in this thermo-active pile test described in this paper.

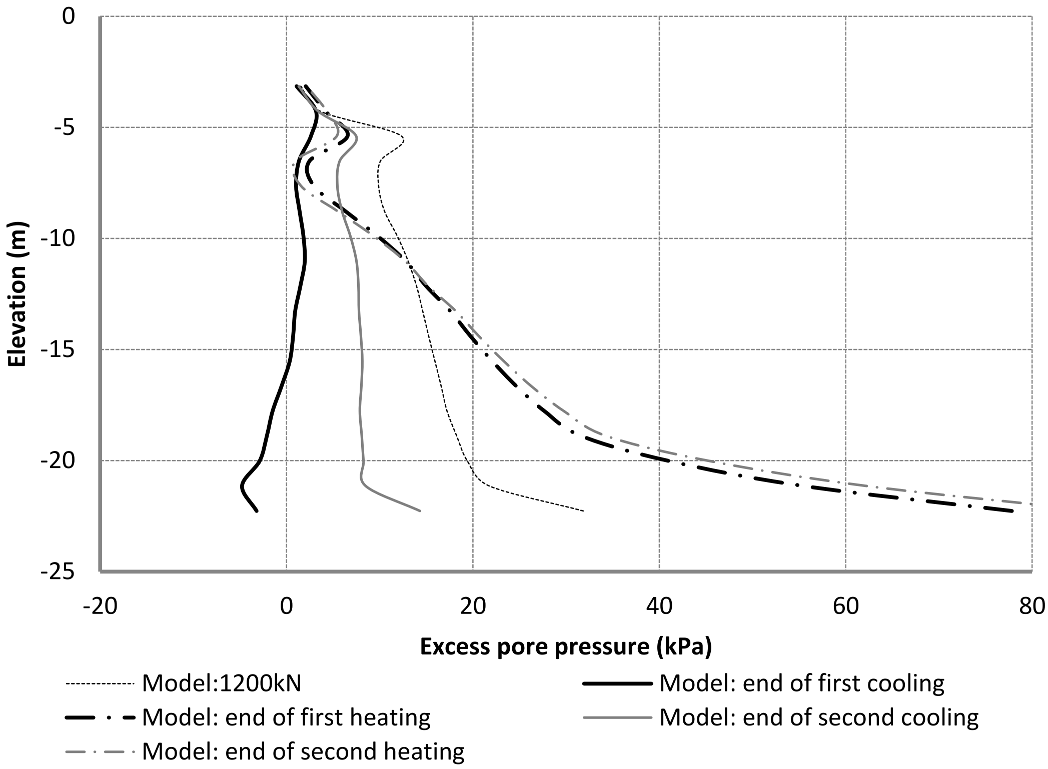

Figure 6. Excess pore pressure in the soil 0.5 m from the pile during cooling and heating cycles

During the first cooling stage, the pore pressure reduced throughout the boundary of the pile and soil due to soil contraction. There was a small negative pore pressure developed. The small perturbation at 5 m depth disappeared because the negative excess pore pressure reduction due to cooling was greater than the original excess pore pressure developed during the mechanical loading. Figure 4 shows the decrease in temperature is quite uniform along the whole thermo-active pile, but the variation between loading only stage and cooling stage increase with pile depth. This is due to the effects of pile-soil interaction. During cooling stage, the lower part of pile additionally moved upwards in the opposite direction of the case under a mechanical load only, but the upper part moved downwards. This thermally induced shear between the pile and the soil caused the decrease in excess pore pressure at bottom, but further increase in the excess pore pressure around top.

The pore pressures increased when the pile was heated. Large excess pore pressure developed at the pile base because the pile bottom was kinematically constrained, indicating that the end bearing contribution to the load bearing increased relative to the shaft contribution. The small perturbation of excess pore pressure at 5m depth observed in the mechanical loading only case disappeared because of upward movement of the upper part of the pile.

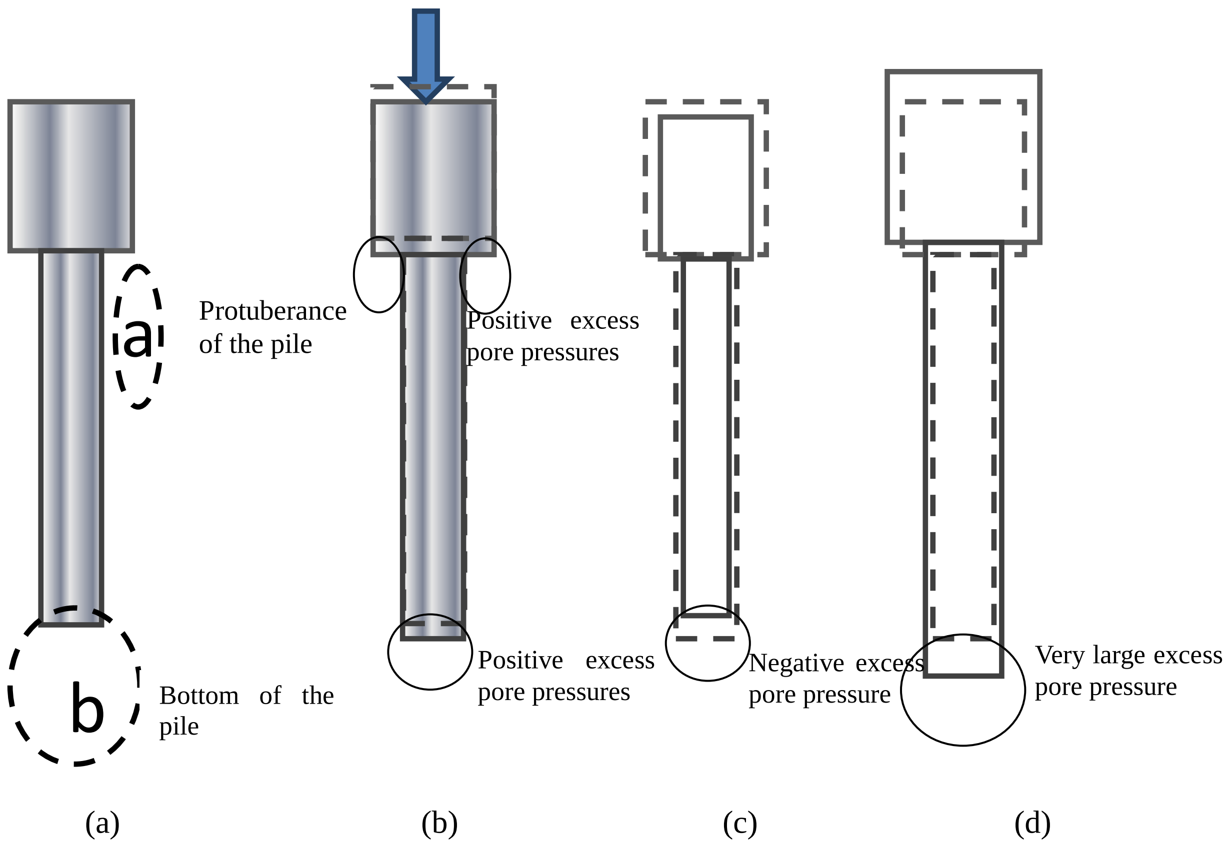

Figure 7. Influence of pile expansion on the neighbouring soil: (a) pile geometry; (b) under physical loading; (c) during cooling; (d) during heating

The computed excess pore pressure with distance from pile center is shown in Figure 8. Under the mechanical load only, a sharp increase in excess pressure from 0kPa to about 18kPa with decreasing distance from the pile was observed, showing the extent of the influence zone by the mechanical load was about 4m. During the first cooling stage, the excess pore pressure around the pile decreased. The largest excess pore pressure was only about 2kPa, but the influence zone spreads a little further from the pile compared to the mechanical loading only case. During the subsequent heating stage, the sharp increase in excess pressure appeared again and the peak value was about 19kPa, but the influence zone was only about 2m, much smaller than the previous cooling stage. This was due to the shorter duration of the heating stage compared to cooling stage.

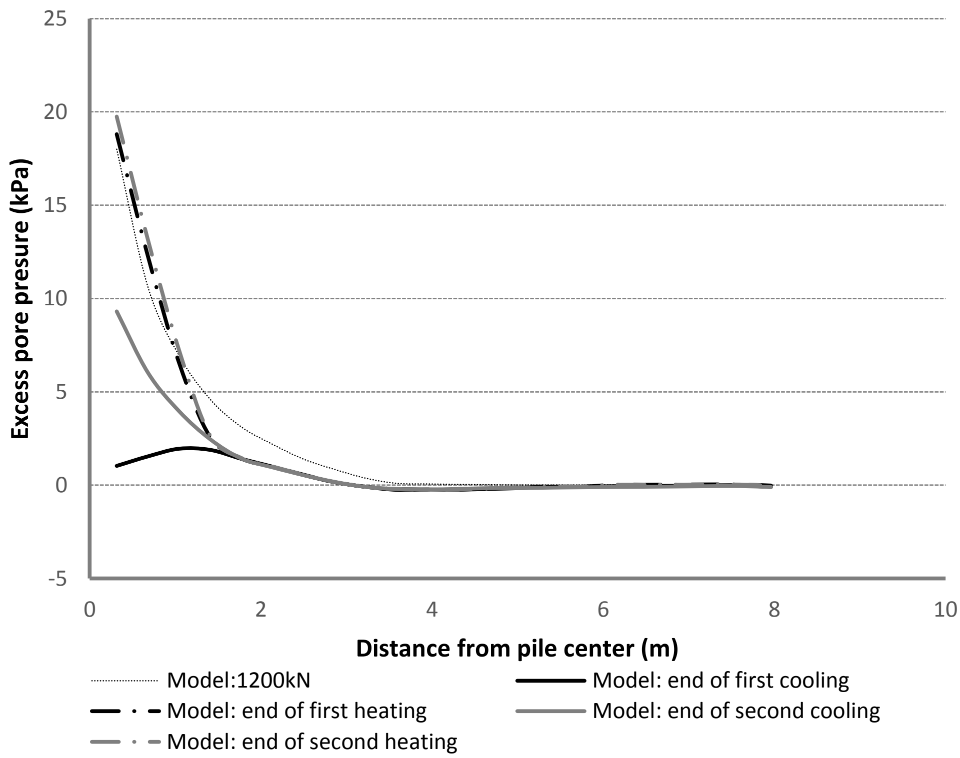

Figure 8. Excess pore pressure with distance from pile center at elevation -12m

5.4 Pile response

Figure 9(a) shows the computed axial stress profiles in the pile during the mechanical loading of 1800 kN and 1200 kN. The profiles were derived from the distributed FO strain data with an assumption that the axial Young's modulus of the pile is 40 GPa. The simulation results are broadly consistent with the monitoring data in terms of the general shape of the stress distribution. Because the upper 5 m of the pile has a larger diameter than the remainder of the pile, the axial stress was about 10% – 20% less than if it had been the same diameter as the remainder. The corner end bearing effect also reduced the axial stress in the pile.

Figure 9(b) shows the axial stress profile in the pile during the first cooling and heating stages. As the pile shrank towards the mid-section, negative incremental friction developed at the lower part of the pile, whereas positive incremental friction developed at the upper part of the pile (Bourne-Webb et al. 2009 and Amatya et al. 2012). This resulted in more friction at the upper part of the pile and a faster decrease in axial stress with depth after cooling, compared to the case with mechanical loading only. The magnitude of the kink at 5 m depth decreased because the pile moved further downwards than the soil did at this location. That is, the corner end bearing effect was reduced. At the lower part of the pile, negative (tensile) incremental stress developed in the pile as the pile shrank upwards.

During the subsequent heating stage, the pile expanded upwards at the upper part and downwards at the middle and lower part. An incremental negative friction developed at the upper part, and hence the maximum axial stress in the pile (6200 kPa) occurred between 6 m and 10 m in depth, and was greater than that applied to the pile head by the physical load. At the mid and lower parts of the pile, additional friction developed and hence the axial stress reduced rapidly with depth. There was a small increase in stress at the bottom because the soil was pushed downwards by the expansion of the pile.

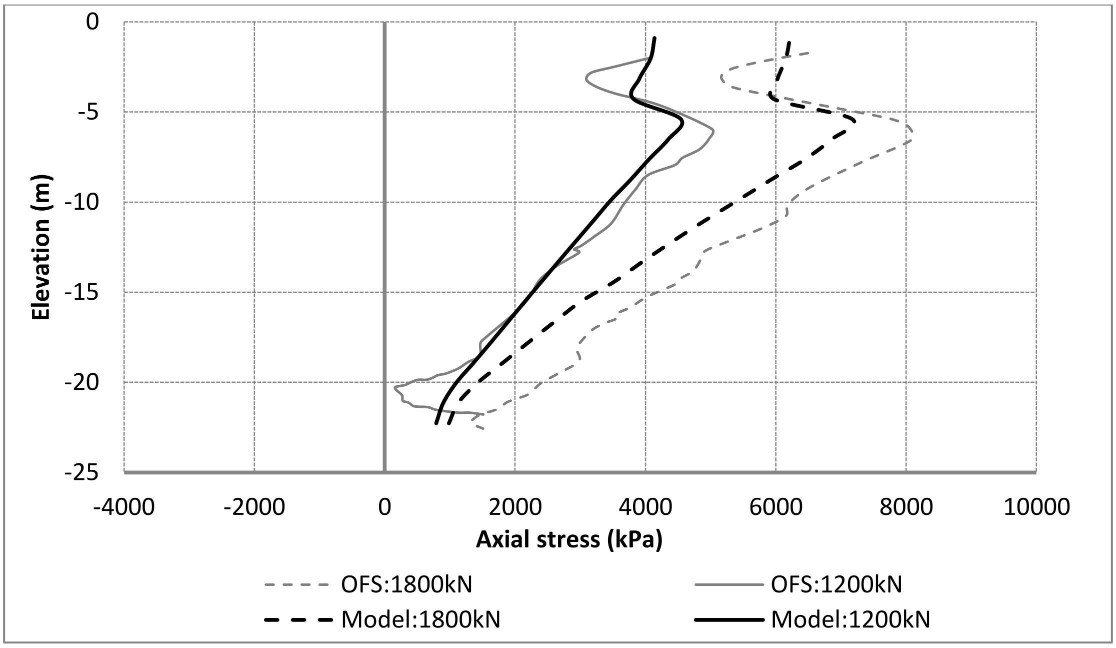

(a)

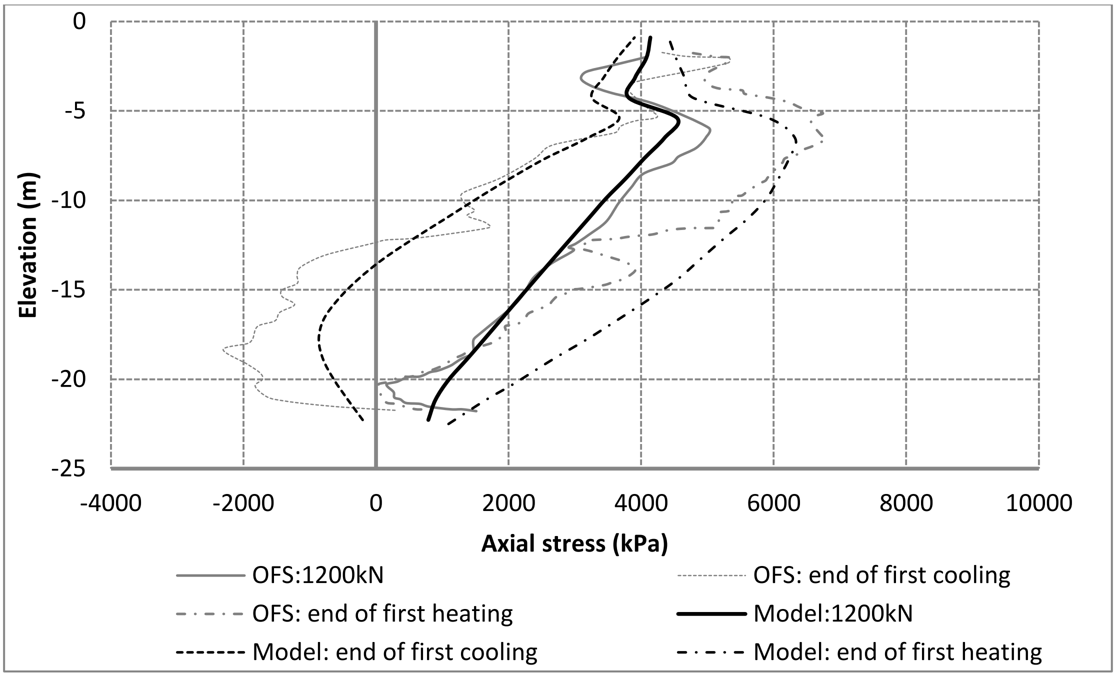

(b)

Figure 9. (a) Change of axial stress in the pile after loading; (b) Axial stress in the pile during the cooling cycle and heating cycle.

5.5 Shear stress development

Figure 10 shows the radial strain profiles of the pile at different stages of the test. When loading to 1200 kN, the radial strain in the pile was quite small, at about -10με~0με (tension positive). When the pile was under a static load, it pushed in the radial outward direction due to the Poisson's ratio effect. In the cooling stage, the pile contracted radially inwards and the radial tensile strain increased to about 155 με–165 με. In the heating stage, the pile expanded and the radial strain decreased to about -100 με—90 με. As shown in Figure 2(b), the pile temperature reduced by about 19℃ in the cooling phase and increased by about 10℃ in the heating phase. Hence, the correlation in Figure 10 indicates that every 1℃ change in temperature generates a change of roughly 8–9 με in the radial strain for the test pile, which is consistent with the thermal expansion coefficient of concrete of 8.5με/°C. However, the maximum radial diameter movement of the pile between the cooling and heating stage was about 70μm, which is very small.

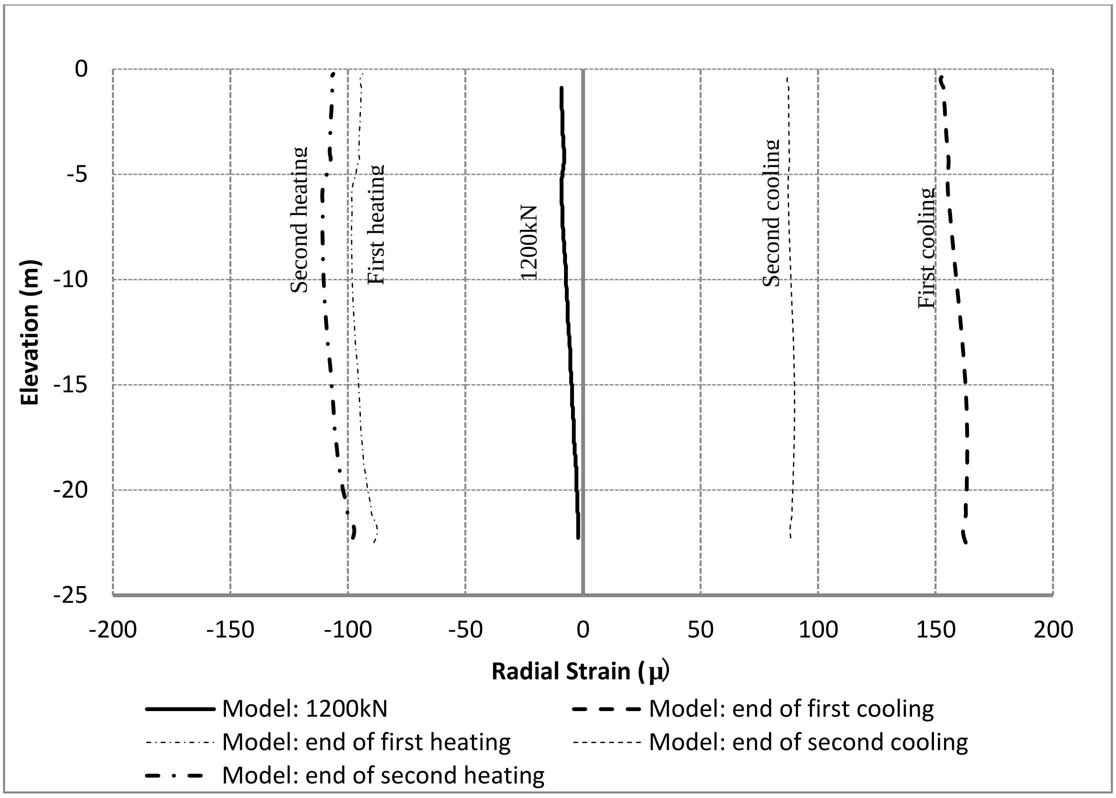

Figure 10. Radial strain of the pile shaft

Figure 11 shows the change in the effective radial stress profile at different stages of the field test along the pile-soil interface. The difference in the effective radial stress between the cooling and heating stages increased with depth. But different from the drained analysis, the magnitude of temperature change didn't correspond to the change in radial effective stress, which was small, at approximately 10 kPa. That is the thermally induced excess pore pressures observed in Figure 6 affect the effective radial stress due to the larger thermal expansion of pore water compared with soil skeleton. The shear stress is governed by the stress reversal behaviour of the cooled or heated soil region next to the pile in relation to the surrounding non-cooled/heated region of the soil.

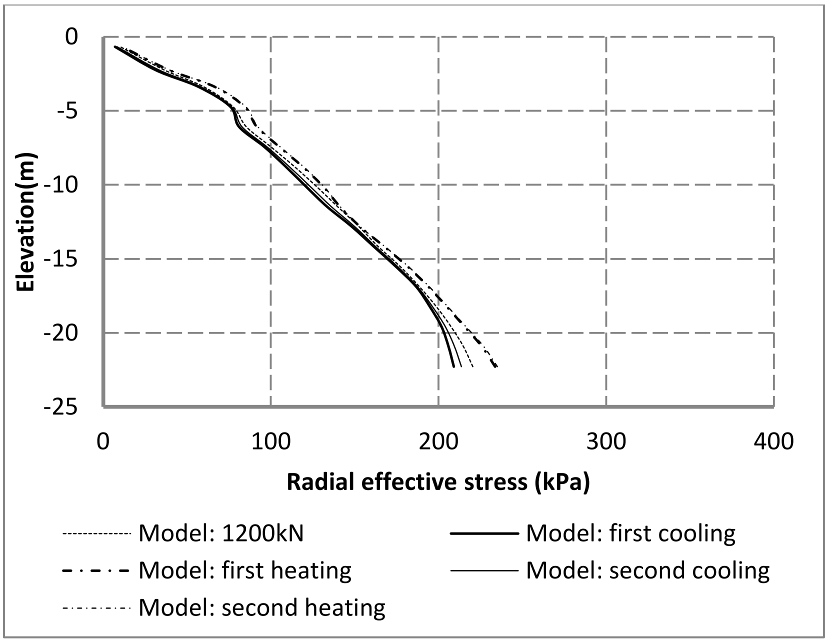

Figure 11. Radial effective stress along the pile for different temperature changes

Figure 12 shows the shear stress profiles along the pile at different stages of the test, in which the shear stress in the soil element next to the pile is plotted. In the 1200 kN mechanical loading only stage, the shear stress was almost constant throughout the depth of London clay because its stiffness increases with depth.

During the cooling stage, the shear stress in the upper part increased due to the pile shrinking downwards, and the relative displacement of the pile and soil near the pile relative to the outer region of the soil was in the same direction as in the mechanical loading only stage. The largest shear stress was about 48 kPa at an elevation of -10 m. In the lower part, the pile shrank upwards and negative incremental shear stress developed. The shear stress decreased, and the smallest shear stress was about -40 kPa at the bottom of the pile.

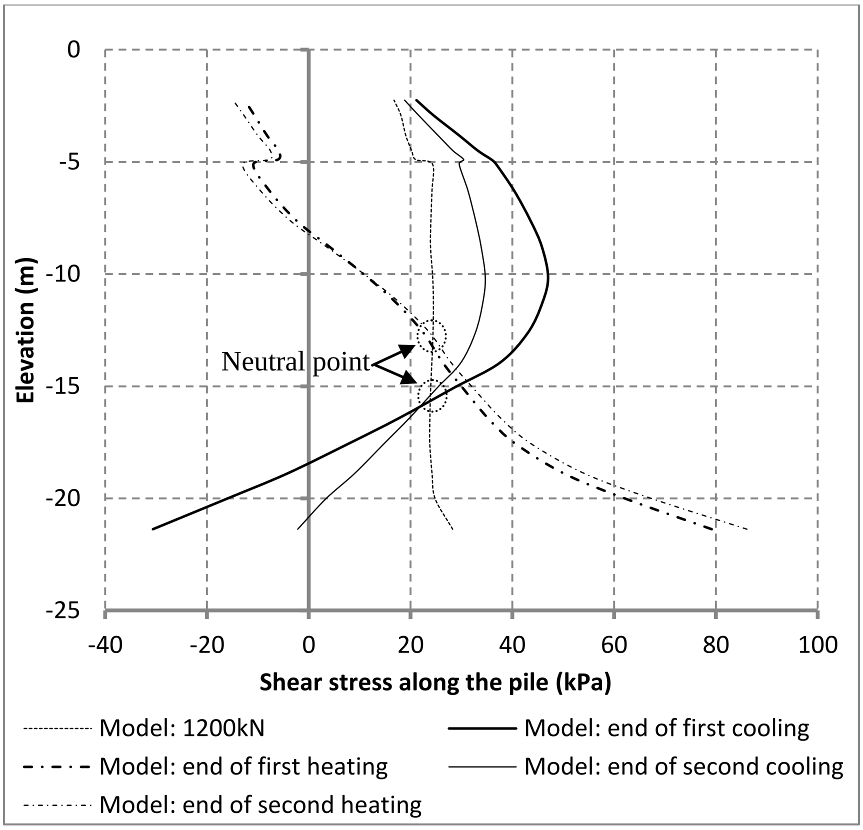

Figure 12. Shear stress along the pile for different temperature changes

Figure 13 shows the shear stress-shear strain plot of a soil element in the upper part of the pile (7 m bgl), and Figure14 shows the same in the lower part (18 m bgl). In the upper part, the shear strain increment was in the same direction as that of the mechanical loading stage. In this particular case, the shear stress reached the ultimate shear stress strength and the load was transferred downward. In the lower part, the thermally induced shear strain was in a different direction to the mechanical loading stress, which meant that the stress remained in the elastic range. Due to the limited shaft resistance developed in the upper part by plastic yielding, the neutral point shows the location where the stress reversal occurred in the lower part of the pile, at 16 m bgl, as shown in Figure 12.

In the subsequent heating stage, the upper part of the pile moved upward, whereas the lower part of the pile moved downward. Stress reversal occurred in the soil next to the pile. The shear stress was smaller than the ultimate shear stress, hence the soil behaviour near pile was non-linear elastic, as shown by the solid lines in Figure 13 and 14. As both parts exhibited elastic-like behaviour, the neutral axis moved upwards to the mid-point of the pile.

In the second cooling and heating stages, the shear stress in the soil element at 7 bgl moved between 25 kPa and -3 kPa, as shown in Figure 13. These are lower than the values in the first cooling and heating cycle because of the heavily overconsolidated nature of the London clay. Similarly, the shear stress in the soil element at 18 m bgl was within the yield stress envelope of the first cycle, as shown in Figure 14. Hence there was no further increase in the overall displacement of the pile by plastic deformation of the clay around the pile. The thermally induced cyclic “elastic-like” pile displacement was approximately 2 mm between the heating and cooling cycles, over a temperature difference of approximately 30 degrees, as shown earlier.

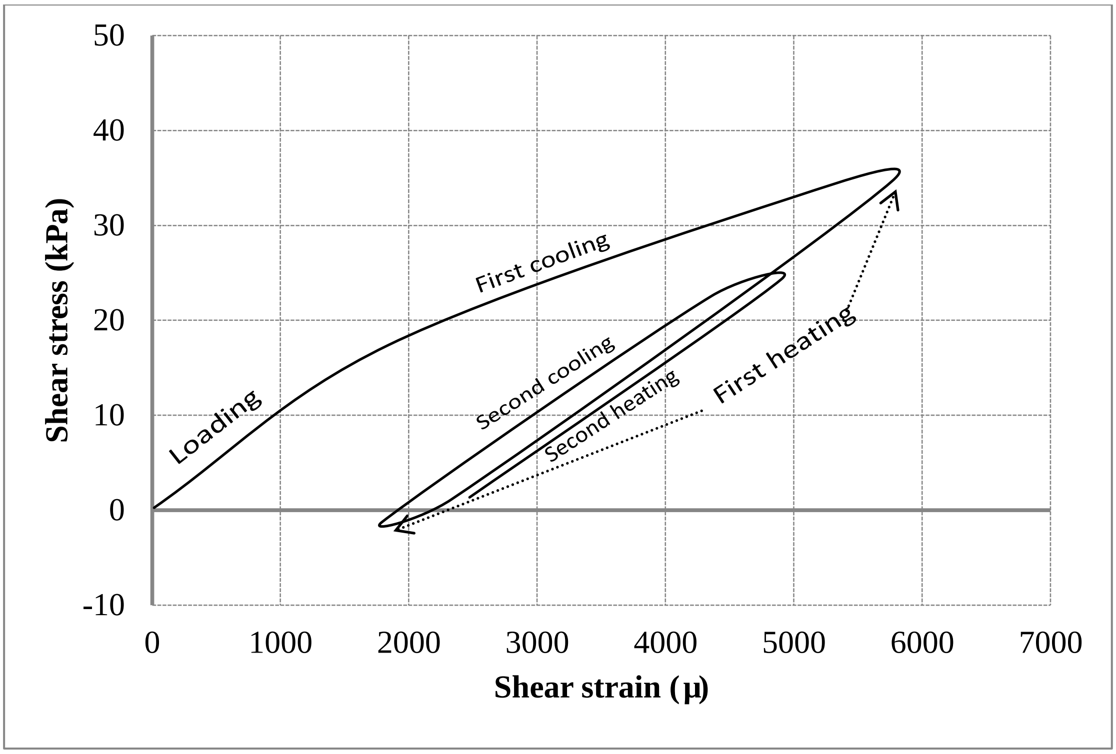

Figure 13. Change of shear stress with shear strain at elevation -7 m

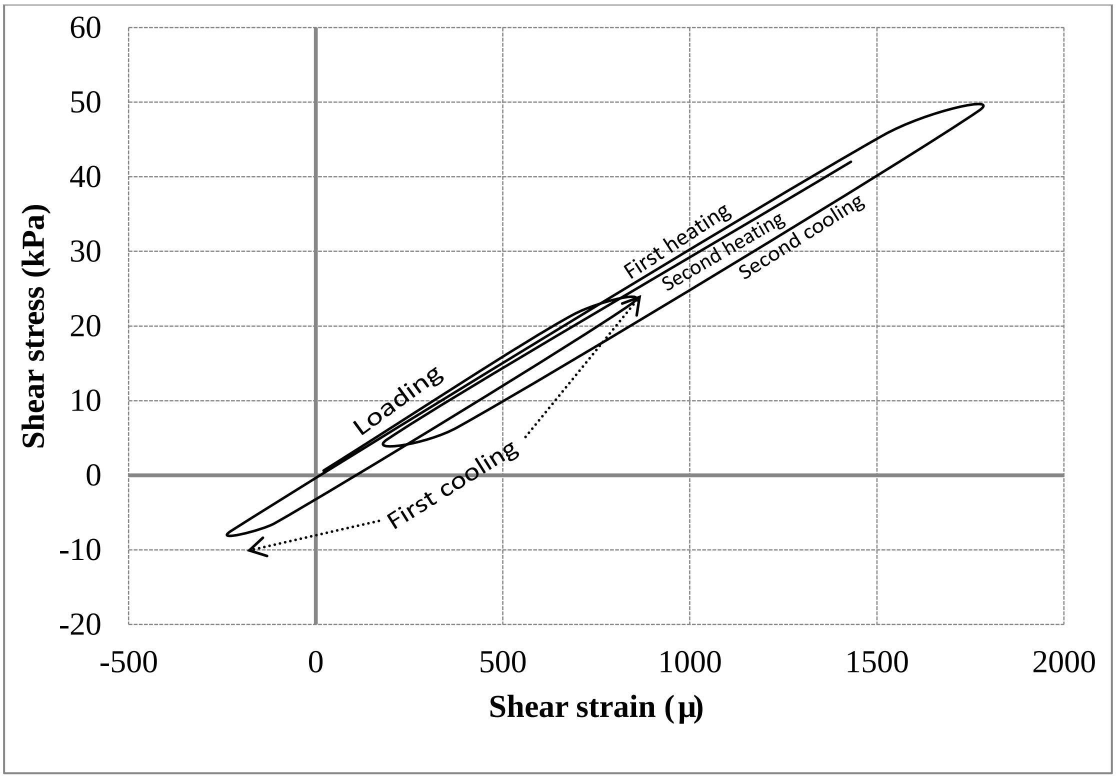

Figure 14. Change of shear stress with shear strain at elevation -18 m

6 Conclusions

The pile-soil interaction behaviour of a thermos-active pile as tested at the Lambeth College field trial (Bourne-Webb et al. 2009) was investigated by conducting a thermo-hydro-mechanical finite element analysis using an advanced soil constitutive model. Negative excess pore pressures were computed around the pile during cooling, whereas positive excess pore pressures developed during heating. This is due to the difference in the thermal expansion coefficients of the pore fluid and the soil skeleton, and the low permeability nature of London clay. There was a difference in the radial effective stress acting on the pile-soil interface between the cooling and heating stages, but the average change along the pile was small (less than 10 kPa). Hence, in this particular case, the pile-soil interaction is governed by the shear mobilization by thermally induced cyclic displacements rather than by changes in the normal effective stress acting at the pile shaft.

During the first cooling stage, the shear stress at a small portion in the upper part of the pile reached close to the yield values, which led to an additional settlement of about 3 mm from the original settlement of 2 mm by the 1200 kN mechanical loading. In the subsequent heating stage, stress reversal occurred at the soil-pile interface, which was behaviour elastic in both the upper and lower parts of the pile. The pile moved upwards by about 2 mm over a temperature change of 30°C. The simulation results show that the mobilized shear stress from the subsequent heating and cooling cycles were much lower than the ultimate friction yield envelope, and hence remained within the elastic region due to the heavily overconsolidated nature of the London clay. The mobilized shear stress from the subsequent heating and cooling cycles under extreme temperatures were much lower than the ultimate friction yield envelope, and remained within the elastic region. Hence there was no further increase in the overall displacement of the pile. The thermally induced cyclic “elastic-like” pile displacement was approximately 2 mm between the heating and cooling cycles, over a temperature difference of approximately 30 degrees.

The thermal cycle loading in the field test was much faster than the actual seasonal operation of the GSHP. The soil-pile interaction of the two cases is expected to be different because the excess pore pressures generated during the heating and cooling will dissipate over time. This may result in changes to the radial effective stress acting at the pile-soil interface. In addition, as the temperature of the ground spreads radially and the excess pore pressure dissipates around the pile, the relative movement between the soil skeleton and the pile becomes smaller since the thermal expansion coefficients are relatively similar. Therefore, the changes in axial stress during short-term thermal loading are expected to diminish with time, which will be the subject of our future study.

Acknowledgement

This research work is funded by the Low Carbon Energy University Alliance of Cambridge University, Tsinghua University and MIT. We thank Professor Kenichi Soga, (UC Berkeley) for comments and guidance that greatly improved the research results.

Notation

β	parameter defining the tilt of the yield surface
p'_0	preconsolidation pressure
ε^p	plastic strain tensor
R	ratio of subloading surface size
C_b	material constants which control the initial gradient of the swelling line
ω_s	non-linearity of the one-dimensional swelling line
p_a	atmospheric pressure
T	soil temperature
ξ	dimensionless distances in space
D	gradient of the isotropic swelling line at the low mean effective pressure
r	constant which controls the rate at which the isotropic swelling line reaches the gradient D
M	gradient of the critical state line

Reference

Abdelaziz S, Ozudogru T Y. Non-uniform thermal strains and stresses in energy piles[J]. *Environmental Geotechnics*, 2016, 3(4): 237-252.

Adam, D., & Markiewicz, R. (2009). Energy from earth-coupled structures, foundations, tunnels and sewers. Géotechnique, 59(3), 229-236.

Amatya, B. L., Soga, K., Bourne-Webb, P. J., Amis, T., & Laloui, L. (2012). Thermo-mechanical behaviour of energy piles. Géotechnique, 62(6), 503-519.

Amis, T., Bourne-Webb, P., Davidson, C., Amatya, B. & Soga, K. (2008). An investigation into the effects of heating and cooling energy piles whilst under working load at Lambeth College, Clapham Common, UK. Proc. 33rd Ann. and 11th Int. Conf. of the Deep Foundations Institute, CD-rom, 10 pages.

Bourne-Webb, P. J., Amatya, B., Soga, K., Amis, T., Davidson, C., & Payne, P. (2009). Energy pile test at Lambeth College, London: geotechnical and thermodynamic aspects of pile response to heat cycles. Géotechnique,59(3), 237.

Bourne-Webb, P. J., Bodas Freitas, T. M., & Freitas Assunção, R. M. (2016). Soil–pile thermal interactions in energy foundations. Géotechnique,66(2), 167-171.

Brandl, H. (2006). Energy foundations and other thermo-active ground structures. Geotechnique, 56(2), 81-122.

Campanella, R. G., & Mitchell, J. K. (1968). Influence of temperature variations on soil behavior. *Journal of Soil Mechanics & Foundations Div*.

Caulk, R., Ghazanfari, E., & McCartney, J. S. (2016). Parameterization of a calibrated geothermal energy pile model. *Geomechanics for Energy and the Environment*, 5, 1-15.

Chen, D., & McCartney, J. S. (2016). Parameters for Load Transfer Analysis of Energy Piles in Uniform Nonplastic Soils. *International Journal of Geomechanics*, 17(7), 04016159.

Di Donna, A., & Laloui, L. (2015). Numerical analysis of the geotechnical behaviour of energy piles. *International Journal for Numerical and Analytical Methods in Geomechanics*, 39(8), 861-888.

Dupray, F., Laloui, L., & Kazangba, A. (2014). Numerical analysis of seasonal heat storage in an energy pile foundation. Computers and Geotechnics, 55, 67-77.

Gao, J., Zhang, X., Liu, J., Li, K. S., & Yang, J. (2008). Thermal performance and ground temperature of vertical pile-foundation heat exchangers: A case study. *Applied Thermal Engineering*, 28(17), 2295-2304.

Ghaaowd, I., Takai, A., Katsumi, T., & McCartney, J. S. (2015). Pore water pressure prediction for undrained heating of soils. *Environmental Geotechnics*, 4(2), 70-78.

GSHP Association. (2012). Thermal pile design, installation and materials standards. Ground *Source Heat Pump Association, National Energy Centre, Davy Avenue, Knowlhill, Milton Keynes, MK5 8NG.*

Hashiguchi, K., & Chen, Z. P. (1998). Elastoplastic constitutive equation of soils with the subloading surface and the rotational hardening. International journal for numerical and analytical methods in geomechanics, 22(3), 197-227.

Knellwolf, C., Peron, H., & Laloui, L. (2011). Geotechnical analysis of heat exchanger piles. Journal of Geotechnical and Geoenvironmental Engineering,137(10), 890-902.

Koene, F. G. H., van Helden, W. G. J., & Romer, J. C. (2000). Energy piles as cost effective ground heat exchangers. In *Proc. TERRASTOCK*.

Laloui, L., & Cekerevac, C. (2003). Thermo-plasticity of clays: an isotropic yield mechanism. Computers and Geotechnics, 30(8), 649-660.

Laloui, L., Nuth, M., & Vulliet, L. (2006). Experimental and numerical investigations of the behaviour of a heat exchanger pile. *International Journal for Numerical and Analytical Methods in Geomechanics*, 30(8), 763-781.

Laver, R.G. (2010). Long-term behaviour of twin tunnels in clay. Ph. D. thesis, University of Cambridge.

Loria, A. F. R., Gunawan, A., Shi, C., Laloui, L., & Ng, C. W. (2015). Numerical modelling of energy piles in saturated sand subjected to thermo-mechanical loads. Geomechanics for Energy and the Environment, 1, 1-15.

Loveridge, F., & Powrie, W. (2014). G-Functions for multiple interacting pile heat exchangers. Energy, 64, 747-757.

McCartney, J.S. and Murphy, K.D. (2017). "Investigation of potential dragdown/uplift effects on energy piles." *Geomechanics for Energy and the Environment*. 1-8. dx.doi.org/10.1016/j.gete.2017.03.001.

NHBC (2010). Efficient design of piled foundations for low-rise housing-Design Guide. Notional House Building Council, Milton Keynes.

Olgun, C.G., Ozudogru, T.Y., Abdelaziz, S.L., and Senol, A. (2014). "Long-term performance of heat exchanger pile groups." *Acta Geotechnica*. 10(5), 553–569.

Pahud, D., & Hubbuch, M. (2007). Measured thermal performances of the energy pile system of the dock midfield at Zürich Airport.

Loria, A. F. R., Gunawan, A., Shi, C., Laloui, L., & Ng, C. W. (2015). Numerical modelling of energy piles in saturated sand subjected to thermo-mechanical loads. *Geomechanics for Energy and the Environment*, 1, 1-15.

Rui, Y. (2014), "Finite Element Modelling of Thermal Piles and walls". Ph. D. Thesis, University of Cambridge.

Saggu, R., & Chakraborty, T. (2015). Cyclic thermo-mechanical analysis of energy piles in sand. *Geotechnical and Geological Engineering*, 33(2), 321-342.

Suckling, T. P., & Smith, P. (2002). Environmentally friendly geothermal piles at Keble College. Oxford, UK, Proceedings of 9th Int. Conf. Exhib. on Piling and Deep Foundation, Nice.

Suryatriyastuti, M. E., Mroueh, H., & Burlon, S. (2014). A load transfer approach for studying the cyclic behavior of thermo-active piles. *Computers and Geotechnics*, 55, 378-391.

Suryatriyastuti, M. E., Burlon, S., & Mroueh, H. (2016). On the understanding of cyclic interaction mechanisms in an energy pile group. *International Journal for Numerical and Analytical Methods in Geomechanics*, 40(1), 3-24.

Wang, W., Regueiro, R. and McCartney, J.S. (2015). "Coupled axisymmetric thermo-poro-elasto-plastic finite element analysis of energy foundation centrifuge experiments in partially saturated silt." *Geotechnical and Geological Engineering*. 33(2), 373-388.

Wongsaroj, J. (2005). Three-dimensional finite element analysis of short and long-term ground response to open-face tunnelling in stiff clay. Ph. D. Thesis, University of Cambridge.

Wongsaroj, J., Soga, K., & Mair, R. J. (2007). Modelling of long-term ground response to tunnelling under St James's Park, London. Géotechnique, 57(1), 75-90.

Yimsiri, S. (2001) “Pre-failure deformation characteristics of soils: Anisotropy and soil fabric.” Ph.D. thesis, Univ. of Cambridge, Cambridge, U.K.